Electrochemical stability and solubility of Ni–Fe–Co ternary alloy oxides in Li/Na carbonate eutectic as an alternative material for MCFC cathodes

Takashi Kudo,[*a] **Kazuhide Kihara,**[b] **Yasunari Hisamitsu,**[b] **Qingchun Yu,**[c]
Mohamed Mohamedi[b] **and Isamu Uchida**[b]

[a]*Research and Development Center, Tohoku Electric Power Co. Inc., 7-2-1 Nakayama
Aoba-ward, Sendai, 981-0952, Japan. E-mail: tkudo@rdc.tohoku-epco.co.jp*
[b]*Department of Applied Chemistry, Graduate School of Engineering, Tohoku University,
07 Aramaki-Aoba, Aoba-ward, Sendai, 980-8579, Japan*
[c]*Institute of Fuel Cell, Shanghai Jiao Tong University, Shanghai 200030, People's Republic
of China*

Electric conductivity, cathodic performance, and stability of Ni–Fe–Co alloy oxides in Li/Na carbonate are
investigated by means of electrochemical measurements and X-ray diffractometry. Higher electrochemical
stability on oxygen reduction was observed with the single-phase oxides of space group $Fm\bar{3}m$, which were
obtained with Co content less than 20 at.% and Ni/Fe/Co = 0.19/0.34/0.47. Electrode impedance measurements
at 1 kHz revealed that the conductivity of the oxides decreased with increasing the amount of Fe. A newly
developed technique for solubility measurements showed that the solubility of Ni^{2+} from Ni–Fe–Co oxides in
Li/Na carbonate decreased with increasing the amount of Fe content. In summary, Ni–Fe–Co complex oxides
consisting of Fe less than 20 at.% and Co less than 20 at.% demonstrate favorable features for MCFC cathode
materials.

Introduction

Internal short-circuiting due to the dissolution of the NiO
cathode[1,2] is commonly recognized as one of the most serious
issues limiting the lifespan of molten carbonate fuel cells
(MCFCs). Thus, alternative materials such as $LiCoO_2$, NiO
supplemented with MgO or Fe_2O_3, or NiO coated with $LiCoO_2$
have been developed to lower the solubility of the cathode.[3,4]
From this viewpoint, we have carried out investigations on
oxygen reduction at *in situ* oxidized metals (*e.g.* NiO,[5–8]
$LiCoO_2$,[9–11] Li_2MnO_3,[11] Ni–Al alloy oxides[12,13]) in carbonate
melts. In this article, we report the electrochemical behavior
and stability of *in situ* oxidized Ni–Fe–Co ternary alloys for
oxygen reduction in Li/Na carbonate eutectic.

$LiCoO_2$ is one of the promising candidate materials because
its solubility is low and its rate of dissolution is slower than that
of NiO. Although the electric conductivity of $LiCoO_2$ is lower
than that of NiO, it can be increased by improved preparation
methods.[14] However, the practical use of $LiCoO_2$ cathodes in
MCFCs is limited by the low mechanical strength and price of
cobalt precursors. $LiFeO_2$ is less expensive than NiO and
$LiCoO_2$, and less soluble in molten carbonate than NiO. On
the other hand, the electric conductivity of $LiFeO_2$ is too
low for practical use in MCFCs. Therefore, Fe based materials
have been employed as an additive for NiO to reduce the
solubility.[15] Bloom *et al.*[16] investigated the resistivity and
cathodic performance of *ex situ* synthesized $NiO–LiFeO_2–$
$LiCoO_2$ solid solutions. The authors reported that adding
$LiCoO_2$ to $LiFeO_2$ is effective at lowering the resistivity of
$LiFeO_2$, and solid solutions of $NiO–LiFeO_2–LiCoO_2$ are
potential alternatives to NiO and $LiCoO_2$ cathodes. However,
the stability of this material in molten carbonate has not been
reported.

To that aim, in this article we report: (*i*) the synthesis and
in situ oxidation of Ni–Fe–Co alloys in $(Li_{0.52}Na_{0.47})_2CO_3$
eutectic investigated with open circuit potential (OCP) and
impedance measurements, (*ii*) the electrochemical performance
towards oxygen reduction of those *in situ* oxidized Ni–Fe–Co
alloys, and (*iii*) their stability in the molten carbonate assessed
with electrochemical and solubility measurements.

Experimental

Electrode preparation and electrochemical measurements

Procedure of melt purification, gas handling, temperature
control, and cell assembly are described elsewhere.[17] Electro-
chemical measurements at elevated pressure were achieved
with a pressurized cell,[6] which is usable up to 5 atm. The
working electrode consisted of a thin layer (0.75 μm thickness)
of Ni–Fe–Co alloy electroplated onto both sides of a gold
substrate (0.39 cm[2]), which was fully immersed in the melt.
We used the Ni–Fe–Co alloy bath developed by Nakamura
et al.[18] for electroplating, which consists of the Permalloy
bath with $NiSO_4$ (Table 1). The thickness of the alloy was
controlled coulometrically at 15 mA cm^{−2}, and then confirmed
by weighing the electrode gain assuming dense plating. Several
compositions were considered. The composition of the alloy
was determined by inductively coupled plasma emission

Table 1 Basic bath composition and its operating conditions for
Ni–Fe–Co ternary alloy plating. Data are cited from ref. 17

$FeSO_4 \cdot 7H_2O$	0.1–0.1 mol dm^{−3}
$CoSO_4 \cdot 7H_2O$	0.0–0.1 mol dm^{−3}
$NiSO_4 \cdot 6H_2O$	0.2, 0.0 mol dm^{−3}
H_3BO_3	0.4 mol dm^{−3}
NH_4Cl	0.28 mol dm^{−3}
Saccharine Na	2 g dm^{−3}
Bath temp.	298 K
Current density	15 mA cm^{−2}
pH	2.8

spectroscopy (ICP, Nippon Jarrell-Ash IRIS 1000, axial photometer) after dissolving alloy samples in 1 M HNO_3. Compositions of all alloys in this paper are expressed in molar fractions. Electrochemical and solubility measurements were conducted at 923 K in $(Li_{0.53}Na_{0.47})_2CO_3$ eutectic (denoted henceforth as Li/Na). The open circuit potential (OCP) and ac impedance at 1 kHz were recorded simultaneously during the oxidation process with a Solartron 1286 potentiostat in combination with a Solartron 1260 frequency response analyzer. The detailed procedure of the OCP and ac impedance measurement is reported elsewhere.[5] All potentials are referred to the standard $(O_2 : CO_2 = 0.33 : 0.67$ atm$)$|Au gas reference electrode denoted henceforth as SOE. Premixed gas mixtures of $O_2 : CO_2 = 9 : 1$ and $O_2 : CO_2 = 2 : 8$ (Sumitomo Seika Chemicals) were used for electrochemical and solubility measurements, respectively. Higher P_{CO_2} in the solubility measurements enables one to accelerate the dissolution process. The total pressure was set at the desired value with a pressure regulator. The phase distribution of the oxides was characterized with a Rigaku RINT-2500 X-ray diffractometer (XRD) equipped with a thin film rotating sample holder using Cu-Kα radiation (0.1540562 nm). The 2θ scan mode with an incident angle of two degrees was employed to obtain thin film XRD profiles.

Solubility measurements

Quantification of oxide solubility in carbonate melts has been commonly conducted according to techniques developed by Ota[19] and Shores,[20] where a sintered or compacted oxide pellet is submerged in the melt, then a melt sample is aspirated with a ceramic tube. However, with this procedure, small particles flaked from the oxide pellet may contaminate the melt sample. The solubility of metal oxides in carbonate melts is reported to be approximately within the 5–50 ppm range.[3,19–26] Thus, even a small amount of oxide particles will result in a large experimental error in such a low solubility range. In this work, we applied thin film alloy samples for solubility measurements, which were prepared according to the same manner as the preparation of the working electrode described in the experimental section. Strip shaped specimens were submerged in the Li/Na carbonate melt held in SSA-S alumina test tubes (Size: od 15 mm, id 12 mm, depth 150 mm, Nikkato-T2). Fig. 1a illustrates the apparatus used for solubility measurements, which is based on the electrochemical cell for atmospheric measurements.[17] This cell can contain up to eight test tubes and enables seven different specimens (including melt composition) to be tested simultaneously. The one remaining tube was used to insert a thermocouple to regulate the temperature. Sampling of the melt was conducted according to the following procedure: (i) a test tube was withdrawn from the cell through an access port with a wire hook after 150 hours of immersion; (ii) the melt sample was taken to a hollow of a colorimetric plate (Nikkato) where it solidified as illustrated in Fig. 1b. At this moment, one can check visually if oxide particles contaminate the melt or not. It took about 100 hours to achieve the equilibrium solubility after immersing test specimens in the melt. Thus, 150 hours of immersion was enough to measure the solubility of Ni^{2+}.

Results

Electrical conductivity of *in situ* oxidation products

The electrical conductivity of the *in situ* oxidation product of Ni–Fe–Co alloy was determined by electrode impedance (series resistance, R_S, measured at 1 kHz) in Li/Na melt at 923 K under $P_{O_2} : P_{CO_2} = 0.9$ atm : 0.1 atm after completion of *in situ* oxidation. The OCP change of a Ni–Fe–Co alloy electrode in Li/Na melt at 923K under $P_{O_2} : P_{CO_2} = 0.9$ atm : 0.1 atm was
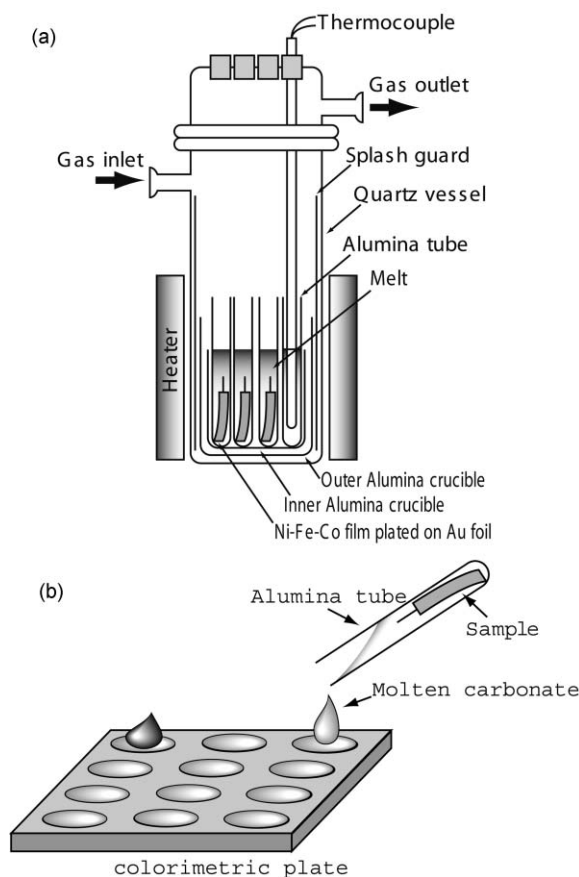

Fig. 1 Schematic illustrations of the apparatus for (a) metal oxide solubility measurements under atmospheric pressure and (b) the manner for molten carbonate sampling.

almost identical to that of non-alloyed Ni.[5,7,27] However, it was found that R_S strongly depended on the alloy composition, particularly on the content of Fe. The correlation between R_S and alloy composition is shown in Fig. 2. Contour diagrams in this paper were plotted by the WaveMetrics IGOR Pro ver. 4 software equipped with a contour-plotting algorithm,[28] which interpolates data to draw smooth contour lines. Differences among R_S values points to differences in conductivities of each oxide for the following reasons. (1) All data were obtained under the same conditions, *i.e.* melt composition, temperature, and surrounding gas composition. (2) Distance and relative location among the working, reference and counter electrodes were always the same in the electrochemical cell. Strictly speaking, R_S is not directly linked to the specific resistance of the oxide, however, it is still effective to compare the behavior of each oxide. The R_S for non-alloyed NiO electrode is reported to be approximately 0.2 Ω cm^2,[5,7,27] which should be regarded as the electrolyte resistance. Thus, values among R_S lower than 0.2 Ω cm^2 would be due to experimental errors. As can be seen from Fig. 2, R_S exhibits values larger than 0.2 Ω cm^2 around 20 at.% of Fe, then increases with increasing the amount of Fe.

Phase distribution of Ni–Fe–Co oxides

Typical XRD profiles of oxidation products are shown in Fig. 3. Single-phase oxides of cubic rock salt structure (space group (s.g.) $Fm\bar{3}m$) were obtained from alloys of lower Co content than *ca.* 20 at.% and Ni/Fe/Co = 0.19/0.34/0.47 (Fig. 3(a), (b)). These are thought to be solid solutions of NiO and α-LiFeO$_2$ as reported by Bloom *et al.*[16] According to the authors,[16] a continuous range of solid solution exists in the NiO–LiFeO$_2$ binary system. With the increase of Co content, one can see another phase of layered rock salt structure (s.g. $R\bar{3}m$) in Fig. 3(c) and (d), which might be a solid solution
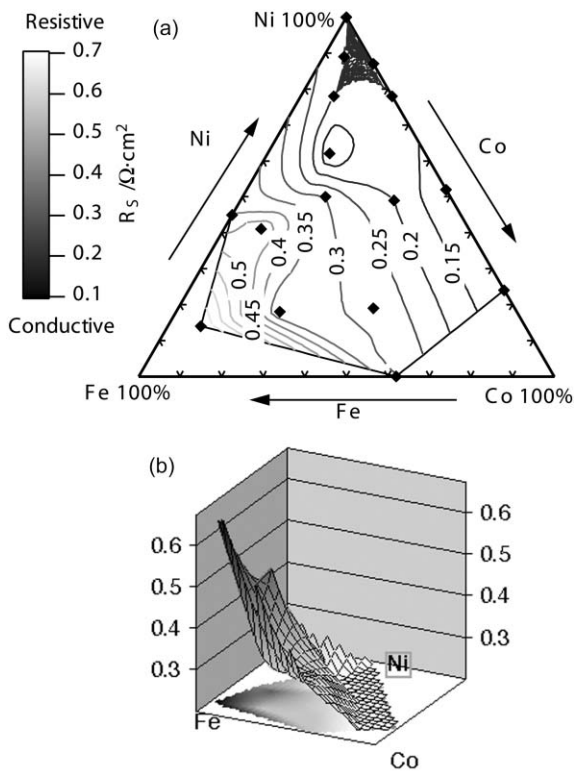
Fig. 2 2D (a) and 3D (b) contour diagrams of R_S of Ni–Fe–Co electrodes oxidized in $(Li_{0.53}Na_{0.47})_2CO_3$ at 923 K under $P_{O_2} : P_{CO_2} = 0.9$ atm : 0.1 atm.

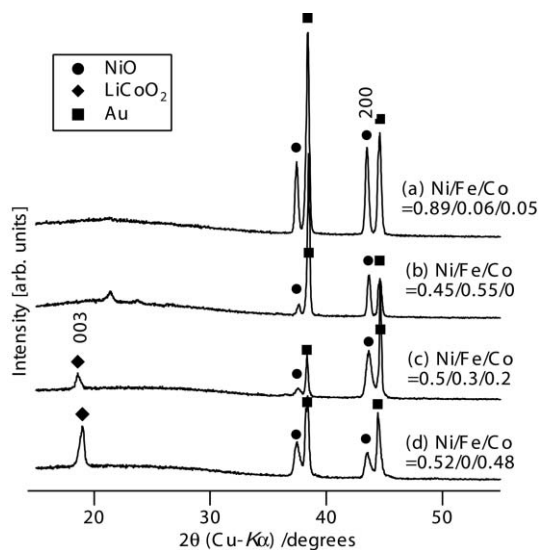**Fig. 3** Thin film XRD profiles of Ni–Fe–Co alloy electrodes oxidized in $(Li_{0.53}Na_{0.47})_2CO_3$ at 923 K under $P_{O_2} : P_{CO_2} = 0.9$ atm : 0.1 atm.

of $LiNiO_2$ and $LiCoO_2$. The phases $Fm\bar{3}m$ and $R\bar{3}m$ are henceforth denoted as NiO and $LiCoO_2$, respectively, for the sake of simplicity. In the following, we will now define "F" as follows:

$$F = \frac{|F_{Fm\bar{3}m}|}{|F_{Fm\bar{3}m}| + |F_{R\bar{3}m}|}$$

where $|F_{R\bar{3}m}|$ and $|F_{Fm\bar{3}m}|$ are the integrated intensities of $LiCoO_2$ 003 and NiO 200, respectively, which are the strongest peaks of each phase. F varies from zero to one in response to the change in phase distribution, *i.e.*, single phase of $R\bar{3}m \Rightarrow$ binary phase of $R\bar{3}m/Fm\bar{3}m \Rightarrow$ single phase of $Fm\bar{3}m$. The value of F by no means indicates the content ratio of NiO and $LiCoO_2$. However, it is still usable to determine which phase
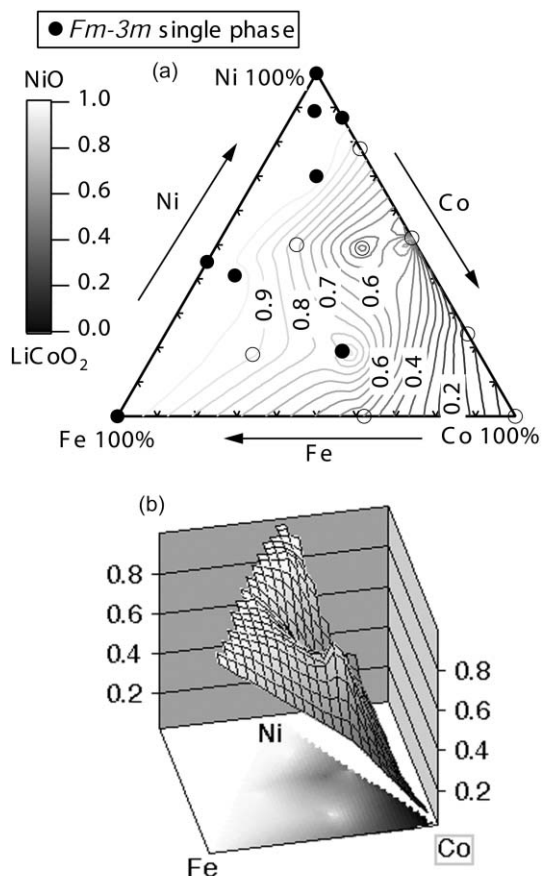
Fig. 4 2D (a) and 3D (b) contour diagrams of the ratio between $|F_{Fm\bar{3}m}|$ and $|F_{R\bar{3}m}|$ obtained from thin film XRD data of Ni–Fe–Co alloy oxide electrodes. Compositions marked by filled circles are identified as single phase of $Fm\bar{3}m$.

is dominant. Fig. 4 shows 2D and 3D contour diagrams of F obtained from thin film XRD data of Ni–Fe–Co alloy oxides. Single phase $Fm\bar{3}m$ was obtained at filled circle markers in Fig. 4a. Bloom *et al.* synthesized solid solutions of NiO, α-$LiFeO_2$, and $LiCoO_2$ *ex situ* by solid-state reaction[16] and characterized the products with XRD. The authors concluded that: (1) NiO and α-$LiFeO_2$ form solid solutions to crystallize in the cubic rock salt structure ($Fm\bar{3}m$) for any Ni/Fe ratio; (2) $LiCoO_2$ and $NiO/LiFeO_2$ form solid solutions retaining the $Fm\bar{3}m$ structure when the Co content is less than approximately 20 at.%. We found that *in situ* oxidized Ni–Fe–Co complex oxides also form solid solutions belonging to s.g. $Fm\bar{3}m$ in the same composition region as Bloom's data.[16] In addition, we found that single phase of $Fm\bar{3}m$ and $Fm\bar{3}m$-dominant oxides ($F > 0.9$) were obtained from Ni/Fe/Co = 0.19/0.34/0.47 and 0.18/0.57/0.25, respectively, which Bloom[16] did not assess.

Stability of Ni–Fe–Co oxides by means of electrochemical measurements

Stability of Ni–Fe–Co alloy oxides was assessed with linear sweep voltammetry at elevated pressure. Degradation of the Ni/Fe/Co = 0.50/0.30/0.20 oxide electrode in Li/Na melt at 3.17 atm is shown in Fig. 5. As seen in Fig. 5, the peak current density of oxygen reduction decreased with time. This decay with time is due to oxide dissolution into the melt and thus a decrease in its surface roughness leading to a lowering of its active surface area. The series of decay rates of i_p is summarized in Table 2, where we categorize oxide samples into three groups according to the decay rate (DR), *i.e.*, (1) DR < 0.005 mA cm^{-2} h^{-1}, (2) 0.05 < DR < 0.01, and (3) 0.01 < DR. Decay rates were calculated from data obtained within 20 hours of immersion. One can see that the compositions of the
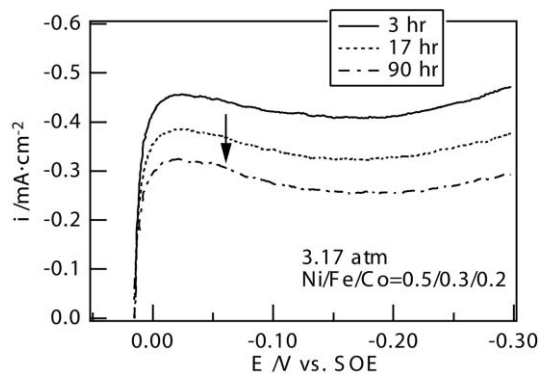
Fig. 5 Variation of oxygen reduction wave with time on Ni/Fe/Co = 0.5/0.3/0.2 alloy oxide electrode under $P_{O_2} : P_{CO_2} = 2.85$ atm : 0.32 atm in $(Li_{0.53}Na_{0.47})_2CO_3$ at 923 K.

samples of slow decay rate have Co contents less than approximately 20 at.%, Ni/Fe/Co = 0.19/0.34/0.47, and 100% Co. The phase distribution (Fig. 4) shows that Ni–Fe–Co oxides in this composition range crystallize with the single phase of $Fm\bar{3}m$ and $R\bar{3}m$, respectively. The large F sample Ni/Fe/Co = 0.18/0.57/0.25 also exhibits a relatively low decay rate (0.007 mA cm^{-2} h^{-1}). Single phase samples would be more stable than binary ones since binary samples will have more grain boundaries, which would trigger the dissolution of oxide particles.

Stability of Ni–Fe–Co oxides by means of solubility measurements

A series of Ni^{2+} solubility from Ni–Fe–Co oxides in Li/Na carbonate at 923 K under $P_{O_2} : P_{CO_2} = 0.2$ atm : 0.8 atm is shown in Table 3. All data were obtained after 150 hours of immersion. Fewer attempts[3,19,23–26] have been made at a systematic study of Ni^{2+} solubility in Li/Na carbonate melt than in Li/K. Fig. 6 shows the solubility of Ni^{2+} dissolved from NiO into Li/Na eutectic at 923 K reported by Fukui,[3,26] Ota,[23] Brenscheidt,[24] and our group.[25] Data of Ota and Brenscheidt were obtained in Ar/CO$_2$ and O$_2$/CO$_2$/N$_2$ atmospheres at P_{Total} = 1 atm, respectively. Data of Fukui were obtained in air/CO$_2$ = 0.7/0.3 up to P_{Total} = 12 atm. As shown in Fig. 6, the data of Fukui and Ota agree well. On the other hand, the data of Brenscheidt and the present work deviate from the others. In particular, the solubility at P_{CO_2} = 0.8 atm measured by us is the lowest in Fig. 6. Our newly developed technique for solubility measurements (Fig. 1b) might result in such low solubility, because this technique eliminates contamination of NiO particles, which causes higher estimations of solubility. We obtain a reaction order of 0.54 that is in agreement with Brenscheidt[25] who reported a reaction order of 0.55. From Fig. 6, the reaction orders of Ota and Fukui were both almost

Table 3 Ni–Fe–Co alloys tested in this work and solubility of Ni^{2+} for each composition under $P_{O_2} : P_{CO_2} = 2.85$ atm : 0.32 atm in $(Li_{0.53}Na_{0.47})_2CO_3$ at 923 K

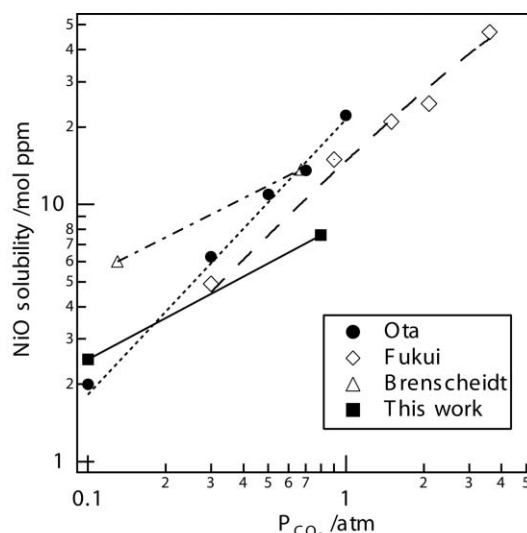| Alloy composition/at.%			Solubility/mol ppm
Ni	Fe	Co	Ni
100	0	0	7.6
56	0	44	9
64	18	18	6
67	33	0	2
60	25	15	2
66	19	15	4
14	77	9	1

Fig. 6 Solubility of Ni^{2+} dissolved from NiO into $(Li_{0.53}Na_{0.47})_2CO_3$ vs. CO$_2$ partial pressure at 923 K. ●: Ota,[23] ◊: Fukui,[3,26] △: Brenscheidt,[24] and ■: this work.

unity. According to our data (Table 3), the solubility of Ni^{2+} from Ni–Fe–Co oxides increased with increasing the amount of Co and decreased with increasing the amount of Fe.

Conclusion

In situ formation and stability of Ni–Fe–Co alloy oxides in Li/Na carbonate eutectic have been investigated. It was found that: (1) conductivity depends on the Fe content strongly. Fe contents higher than 20 at.% lower the conductivity of the oxide; (2) Ni–Fe–Co oxides crystallize with the single phase cubic rock salt structure (s.g. $Fm\bar{3}m$) from lower Co contents than approximately 20 at.% and Ni/Fe/Co = 0.19/0.34/0.47;

Table 2 Compositions of Fe–Co–Ni alloy oxide electrodes classified by the decay rate of peak current density of LSV for oxygen reduction under $P_{O_2} : P_{CO_2} = 2.85$ atm : 0.32 atm in $(Li_{0.53}Na_{0.47})_2CO_3$ at 923 K

(1) Slow decay rate			(2) Medium decay rate			(3) Quick decay rate		
DR < 0.005 mA cm^{-2} h^{-1}			DR = 0.005–0.01 mA cm^{-2} h^{-1}			DR > 0.01 mA cm^{-2} h^{-1}		
Ni (%)	Fe (%)	Co (%)	Ni (%)	Fe (%)	Co (%)	Ni (%)	Fe (%)	Co (%)
45	55	0	18	57	25	24	0	76
50	30	20	52	0	48	0	38	62
41	50	9	87	0	13	49	14	37
0	0	100				78	0	22
19	34	47				62	23	15
14	77	9						
77	15	8						
100	0	0						
89	6	5						

(3) measurements of peak current density coupled with XRD revealed that the single-phase oxide samples exhibit higher stability than $Fm\bar{3}m/R\bar{3}m$ binary samples; (4) solubility of Ni^{2+} decreased with increasing the amount of Fe. Summarizing the above results, Ni–Fe–Co complex oxides with Fe content less than 20 at.% and Co content less than 20 at.% are promising alternative cathode materials for MCFCs.

References

1   Y. Mugikura, K. Shimazu, T. Watanabe, Y. Izaki, T. Abe, H. Urushibata, H. Maeda, K. Sato and T. Murahashi, *Denki Kagaku (presently Electrochemistry)*, 1992, **60**, 117–123.
2   H. R. Kunz and J. W. Pandolfo, *J. Electrochem. Soc.*, 1992, **139**, 1549–1556.
3   T. Fukui, H. Okawa and T. Tsunooka, *J. Power Sources*, 1998, **71**, 239–243.
4   K. Takizawa and A. Hagiwara, *Electrochemistry*, 2001, **69**, 692–698.
5   T. Nishina, K. Takizawa and I. Uchida, *J. Electroanal. Chem.*, 1989, **263**, 87–96.
6   K. Yamada, T. Nishina, I. Uchida and J. R. Selman, *J. Electrochim. Acta*, 1993, **38**, 2405–2411.
7   P. Tomczyk, H. Sato, K. Yamada, T. Nishina and I. Uchida, *J. Electroanal. Chem.*, 1995, **391**, 125–132.
8   M. Mohamedi, Y. Hisamitsu, K. Kihara, T. Kudo, T. Itoh and I. Uchida, *J. Solid State Electrochem.*, 2001, **5**, 538–545.
9   K. Yamada and I. Uchida, *Chem. Lett.*, 1994, 299–302.
10   P. Tomczyk, H. Sato, K. Yamada, T. Nishina and I. Uchida, *J. Electroanal. Chem.*, 1995, **391**, 133–139.
11   K. Yamada, N. Sato, T. Fujino, M. Nishizawa and I. Uchida, *Electrochemistry*, 1999, **67**, 68–71.
12   M. Mohamedi, Y. Hisamitsu, K. Kihara, T. Kudo, T. Itoh and I. Uchida, *J. Alloys. Compd.*, 2001, **315**, 224–233.
13   T. Kudo, Y. Hisamitsu, K. Kihara, M. Mohamedi and I. Uchida, *J. Appl. Electrochem*, 2002 , in press.
14   K. Ota, Y. Takeishi, S. Shibata, H. Yoshitake and N. Kamiya, *J. Electrochem. Soc.*, 1995, **142**, 3322–3326.
15   M. Motohira, T. Sensou, K. Yamauchi, N. Kamiya and K. Ota, *Proc. of the 3rd International Fuel Cell Conference, Nagoya*, ed. I. Uchida, FCDIC, Tokyo, 1999, pp. 239–240.
16   I. Bloom, M. T. Lanagan, M. Krumpelt and J. L. Smith, *J. Electrochem. Soc.*, 1999, **146**, 1336–1340.
17   I. Uchida, Y. Mugikura, T. Nishina and K. Itaya, *J. Electroanal. Chem.*, 1986, **206**, 241–252.
18   A. Nakamura, M. Takai, K. Hayashi and T. Ohsaka, *J. Surface Finishing Soc. Jpn.*, 1996, **47**, 934–938.
19   K. Ota, S. Mitsushima, S. Kato, S. Asano, H. Yoshitake and N. Kamiya, *J. Electrochem. Soc.*, 1992, **139**, 667–671.
20   M. L. Orfield and D. A. Shores, *J. Electrochem. Soc.*, 1988, **135**, 1662–1668.
21   K. Yamada and I. Uchida, *J. Electroanal. Chem.*, 1995, **385**, 57–61.
22   C. G. Lee, K. Yamada, T. Nishina and I. Uchida, *J. Power Sources*, 1996, **62**, 145–147.
23   K. Ota, S. Kato, S. Mitsushima and N. Kamiya, *Denki Kagaku (presently Electrochemistry)*, 1989, **57**, 430–433.
24   Th. Brenscheidt, F. Nitschké, O. Söllner and H. Wendt, *Electrochim. Acta*, 2001, **46**, 783–797.
25   M. Mohamedi, Q. Yu, K. Kihara, Y. Hisamitsu, T. Kudo, I. Ito, M. Umeda, I. Uchida and J. R. Selman, *Proceedings of the 6th International Conference on Molten Salt Chemistry and Technology, Shanghai*, ed. C. Nianyi and Q. Zhiyu, Shanghai University Press, Shanghai, 2001, pp. 235–240.
26   T. Fukui, unpublished data, Japan Fine Ceramics Center, 2002.
27   T. Kudo, Y. Hisamitsu, K. Kihara, M. Mohamedi and I. Uchida, *J. Power Sources*, 2002, **104**, 272–280.
28   W. V. Snyder, *ACM Trans. Math. Softw.*, 1978, **3**, 290–294.